XVIII Brazilian Conference on Soil Mechanics and Geotechnical Engineering
The Sustainable Future of Brazil goes through our Minas
COBRAMSEG 2016 – 19-22 October, Belo Horizonte, Minas Gerais, Brazil

A Computer Program for Integrating Probabilistic 3D Unsaturated Flow Simulations and Numerical Limit Analysis

Guilherme José Cunha Gomes
Pontifícia Universidade Católica do Rio de Janeiro (PUC-Rio), Brazil, guilhermejcg@yahoo.com.br

Jasper Alexander Vrugt
University of California, Irvine, California, USA, jasper@uci.edu

Julia de Toledo Camargo
Stanford University, Stanford, California, USA, juliatcamargo@gmail.com

Eurípedes do Amaral Vargas Jr.
Pontifícia Universidade Católica do Rio de Janeiro (PUC-Rio), Brazil, vargas@puc-rio.br

Raquel Quadros Velloso
Pontifícia Universidade Católica do Rio de Janeiro (PUC-Rio), Brazil, raquelvelloso@puc-rio.br

Alonso Joaquim Juvinao Carbono
Pontifícia Universidade Católica do Rio de Janeiro (PUC-Rio), Brazil, aljuvinao@hotmail.com

SUMMARY: We develop a Monte Carlo framework to integrate a three-dimensional finite element variably-saturated flow model and numerical limit analysis to evaluate the impact of uncertainty about bedrock surface and soil hydraulic parameters on the stability of slopes. In this paper, we explore the main capabilities of our MATLAB program, including pre- and post-processing tools. Pre-processing tools include automatic mesh generation and explicit treatment of uncertainty in key inputs of geotechnical stability models for unsaturated soils. Processing tools are illustrated with three case studies that explore the effectiveness of our methodology. Post-processing tools embrace plots of the factor of safety uncertainty, pressure head distributions and failure mechanisms.

KEYWORDS: bedrock depth, hydraulic parameters, slope stability, unsaturated flow, limit analysis, factor of safety.

1 INTRODUCTION

The stability of a slope is commonly expressed with a quantitative metric named factor of safety (FS). Depending on the geotechnical stability method adopted one can calculate FS in different ways. Generally, slope failure (FS is smaller than unity) will be imminent if equilibrium can no longer be maintained in the slope. On the contrary, when FS is larger than one the slope is considered safe. Thus, the smaller the value of FS, the less stable a hillslope is, and the more susceptible this slope is to failure. One should be particularly careful, however with the interpretation of deterministic FS values, as the different variables that go into its calculation are subject to uncertainty and cannot be measured precisely (Duncan and Wright, 2005).

Probabilistic methods for stability analysis allow the designer to address issues beyond those that can be dealt with deterministic methods. These approaches allow us to calculate confidence intervals of the FS in response to uncertainty in soil properties, measurement data, stratigraphic conditions and model structural errors. Examples of uncertainties in soil properties and stratigraphic conditions include, respectively, the variability of the soil hydraulic prop-

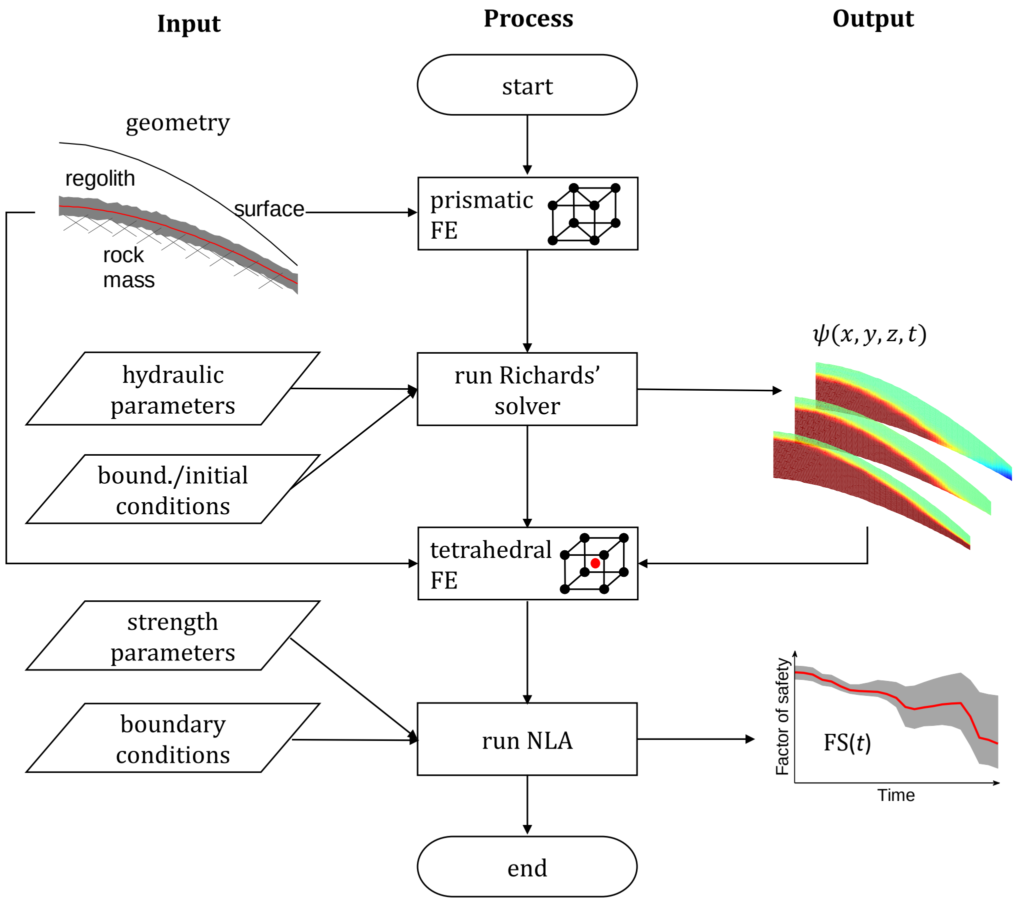

Figure 1: Basic building blocks of the developed MATLAB code for integrating unsaturated flow simulations and numerical limit analysis. Input/output and the main steps of the process are indicated. The code is specially designed to execute Monte Carlo simulations for evaluation of bedrock depth and soil hydraulic parameters uncertainties.

erties and the uncertainty of the bedrock surface.

The purpose of this paper is to present a computer program specially designed to evaluate the impact of bedrock depth variability and soil hydraulic parameters uncertainty on slope stability analysis, and its impact on the probability of failure. To achieve this goal, a three-dimensional finite element solver of Richards' equation (Micheletto, 2008) is coupled with a numerical limit analysis code (Camargo et al., 2016), providing several benefits of an integrated toolbox. As an illustration, we apply our method to a natural hillslope in Rio de Janeiro, Brazil. We emphasize the coordinated impact of both sources of uncertainty (bedrock depth and soil hydraulic properties) on the confidence intervals of the FS. The framework presented herein provides a basis for reliability analysis of geotechnical hazards.

2 MODELING FRAMEWORK

We have developed an integrated framework for stochastic slope stability analysis (Figure 1). This probabilistic framework couples a Monte Carlo algorithm with a three-dimensional variably-saturated flow simulator and a numerical limit analysis (NLA) code. The Monte Carlo algorithm is used to quantify the impact of bedrock depth and soil hydraulic uncertainty on the simulated FS values by repeated numerical simulation of the Richards' solver and NLA codes for the experimental hillslope under investigation.

Our framework is coded in MATLAB and integrates both numerical models so that users do

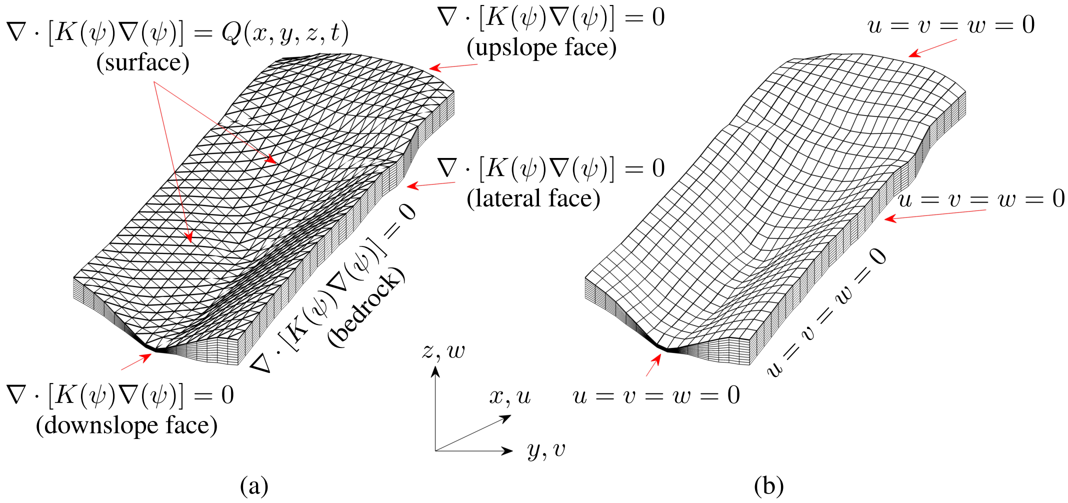

Figure 2: Examples of FE meshes with (a) prismatic and (b) tetrahedral elements for our experimental hillslope. (a) The boundary conditions of the variably-saturated flow model are listed at the edges of the mesh of our flow domain. A precipitation boundary condition, $Q(x, y, z, t)$ is used at the surface of our structured mesh, whereas a no flow condition, $\nabla \cdot [K(\psi)\nabla(\psi)] = 0$ is assumed at the soil-bedrock interface, and at the upslope, lateral and downslope faces of the hillslope domain. (b) The boundary conditions of NLA are separately listed at the edges of the mesh with tetrahedral elements. The symbols u, v and w are used to denote the strain velocities in the directions of the three spatial coordinates, x, y, and z of the hillslope, respectively. Their values follow from the assumed boundary conditions (no velocity: $u = v = w = 0$).

not have to port data from one model to the next. This simplifies considerably slope stability analysis. What is more, the MATLAB code generates automatically prismatic and tetrahedral finite element meshes for the spatial domain of the hillslope of interest and has built-in pre-processing and post-processing capabilities to help setup the models and visualize the results.

A summary of our computer code is depicted in Figure 1. Four basic inputs are required to run the code: slope geometry (including spatially distributed depth to bedrock), soil hydraulic parameters, boundary/initial conditions and strength parameters. Other (optional) inputs include parallel computing, mesh refinement settings and strings that enable Monte Carlo simulations for ensembles of bedrock surfaces and soil hydraulic parameters. The flow model solves Richards' equation and calculates transient values of the pressure head, $\psi(x, y, z, t)$, as function of spatial coordinates (x, y), depth (z) and time (t). ψ nodal values are then interpolated for each element of the FE mesh with tetrahedral elements (red dot symbol of the tetrahedral FE mesh in Figure 1). We refer to the work of Micheletto (2008) for further information on the variably-saturated model used herein. The NLA code, detailed in Camargo et al. (2016), returns the corresponding (transient) values of the FS and velocity vectors at collapse.

In the following sections, we will show the basic building blocks of the developed MATLAB code.

3 PRE-PROCESSING TOOLS

3.1 FE mesh generation

Finite element (FE) meshes with prismatic and tetrahedral elements (see Figure 2) are automatically derived to run the Richards' solver and the NLA code, respectively. Unfortunately, one cannot build the surface mesh without adequate knowledge of the surface and bedrock topographies. The MATLAB toolbox developed herein allows the user to define the density of the surface mesh (number of nodes/elements). What is more, the toolbox also allows the user to define the number of nodes in the z (vertical) direction between the hillslope surface and bedrock.

3.2 Tools for bedrock surface treatment

If desired by the user to investigate the effect of uncertainty about bedrock surface, plausible maps of soil-bedrock interface should be provided. These maps, stored in matrices, are used in our probabilistic framework.

For instance, in a recent paper published by Gomes et al. (2016b) we have developed a geomorphologic model for the spatial distribution of depth to bedrock (DTB) using high-resolution topographic data, numerical modeling and Bayesian analysis. In summary, we have reconciled the simulated bedrock depths of our model with field observations (Gomes et al., 2016a) using Bayesian analysis with the DREAM algorithm (Vrugt, 2016). This approach uses Markov chain Monte Carlo Simulation (MCMC) simulation with DREAM to search efficiently the model parameter space in pursuit of posterior samples that statistically best honor the bedrock depth. Our results demonstrated that our DTB model predicted accurately the observed soil-bedrock interface data. The posterior mean DTB simulation was shown to be in good agreement with the measured data.

In this paper, we illustrate our method by sampling bedrock topography maps from the posterior prediction uncertainty of the DTB model and propagate these maps forward through the computer code developed herein to derive probabilistic estimates of the FS.

The user, however, can use different approaches to derive bedrock maps with uncertainty estimates, for instance, kriging, linear/nonlinear regression, etc.

Figure 3 displays an overview of the hillslope under investigation, and presents a three-dimensional plot (with colorbar) of the posterior mean bedrock depth simulated by the DTB model (top panel), and a graph of the mean posterior bedrock depth (red line) of the transect **CC**' predicted by the DTB model in the bottom plot (see Gomes et al. (2016a) for spatial location). The dark and light gray region in this graph plot the 95% prediction intervals of the DTB model due to parameter and total (model + parameter) uncertainty.

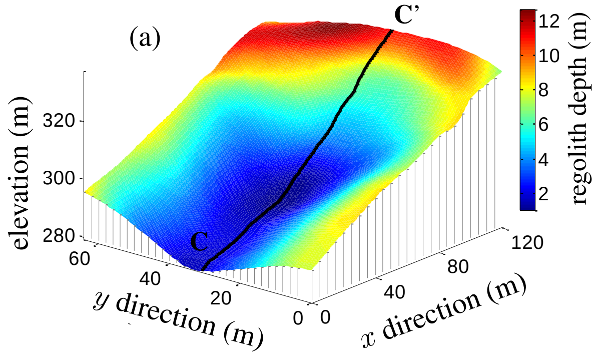

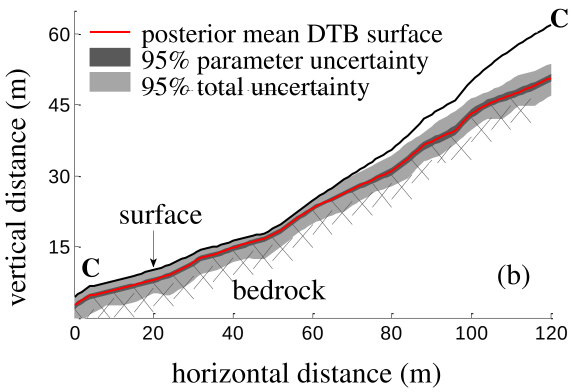

Figure 3: Distribution of the bedrock depth in the investigated slope: (a) regolith depth predicted with the posterior mean solution derived using Bayesian analysis; (b) transect **CC**' of the central part of the slope showing the mean (red line), 95% confidence intervals due to parameter (dark gray) and total uncertainty (light gray).

The posterior mean bedrock depth map is computed from the posterior parameter solutions derived from the DREAM algorithm. If we write the DTB model, $\mathcal{F}$ as follows

$$\mathbf{H} = \mathcal{F}(\boldsymbol{\delta}), \tag{1}$$

then $\mathbf{H}$ signifies the simulated bedrock depth map for the parameter values $\boldsymbol{\delta} = \{\delta_1, \ldots, \delta_d\}$. We can now store the posterior sample of parameter vectors in the $M \times d$ matrix $\boldsymbol{\Delta} = \{\boldsymbol{\delta}_1, \ldots, \boldsymbol{\delta}_M\}$. These samples can be evaluated by the DTB model and used to produce an ensemble of M different bedrock depth maps, $\boldsymbol{\hbar} = \{\mathbf{H}_1, \ldots, \mathbf{H}_M\}$. The expected value of these maps, $\mathbb{E}(\boldsymbol{\hbar})$ constitutes the posterior mean bedrock depth map of Figure 3 (a). The variations in bedrock depth of the M samples defines the posterior prediction uncertainty of the DTB model, plotted in 3 (b) for the **CC**' transect.

3.3 Tools for hydraulic properties uncertainty

Table 1 lists the mean values of the soil hydraulic parameters (fourth column), their standard deviation (fifth column), and linear correlation coefficients (last five columns) required by the program to simulate uncertainty estimates of FS due to soil hydraulic parameters.

The values of the hydraulic properties listed in Table 1 are derived from the ROSETTA program (Schaap et al, 2001) using the methodology developed by Scharnagl et al (2011). The ROSETTA program implements hierarchical pedotransfer functions to estimate the van Genuchten-Mualem (VGM) parameters from basic soil data, such as textural class. The procedure adopted here can be summarized in four steps: (1) drawn a random sample of input variables (textural data); (2) use ROSETTA to generate the corresponding random sample of soil hydraulic parameters; (3) calculate the correlation matrix of the random sample of soil hydraulic parameters; and (4) derive the full covariance matrix of the predicted soil hydraulic parameters.

A detailed description of these four steps appears in Scharnagl et al (2011) and thus will not be repeated herein. In this paper, the random sample of input variables (step 1) was obtained from 52 measured sand, silt and clay percentages ($\boldsymbol{f}$) of different soil layers at the experimental site of Figure 3 (Gomes et al., 2016a). This ensemble was then used to estimate the mean ($\boldsymbol{\mu_f}$) and standard deviation ($\boldsymbol{\Sigma_f}$) of the measured textural data. The random sample of input variables was generated from a normal distribution, $\mathcal{N}(\boldsymbol{\mu_f}, \boldsymbol{\Sigma_f})$. The remaining steps (2 to 4) follows exactly the approach by Scharnagl et al (2011). The resulting full covariance matrix $\Sigma_{\boldsymbol{p}}$ accounts for parameter uncertainty and correlation induced by the pedotransfer function. The mean parameter values ($\boldsymbol{\mu_p}$) and the correlation matrix are shown in Table 1.

Representing one of the pre-processing outcomes of our code, Figure 4 illustrates how the multivariate normal distribution affects the confidence intervals of the water retention and hydraulic conductivity functions. The red line denotes the mean parameter values, whereas the 95% confidence intervals due to parameter uncertainty are depicted in gray. The confidence intervals around the inflection point of the water retention function (Figure 4 (a)) reduces symmetrically, but the uncertainties in the wet and dry ranges are poorly affected. This behavior reflects the parameter correlation considered in the prior distribution and agrees with the soil-water characteristic curve reported by Scharnagl et al. (Scharnagl et al, 2011). The hydraulic conductivity function (Figure 4 (b)) shows a larger uncertainty in the wet range due to the variability in the saturated permeability, K_s, whereas in the dry range the confidence interval is smaller.

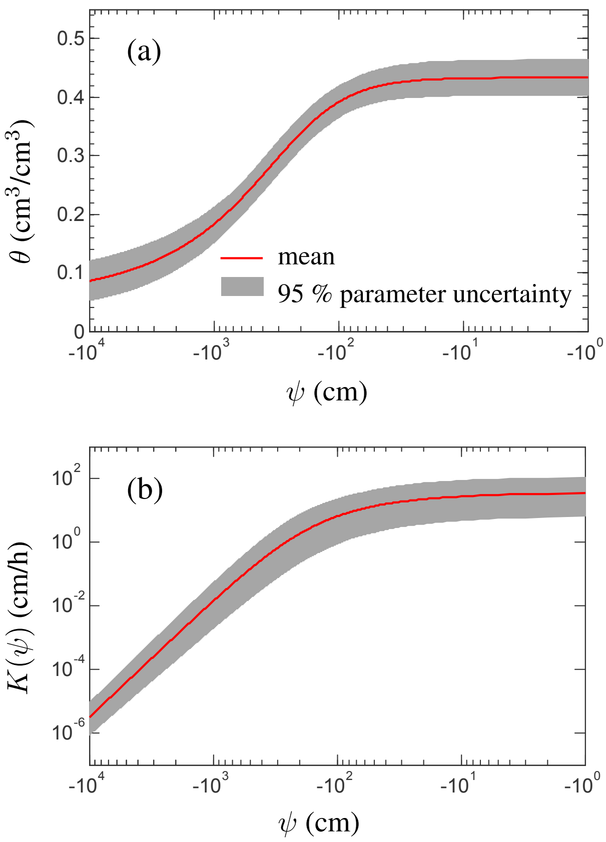

Figure 4: 95% prior uncertainty bounds of (a) the water retention function and (b) the hydraulic conductivity function corresponding to the multivariate normal distribution with correlation among the soil hydraulic parameters. Red lines in both plots correspond to the mean values.

4 PROCESSING CAPABILITIES

In this section, we use three different case studies to summarize our processing capabilities and to

Table 1: Mean values, standard deviations and correlation coefficients of the ROSETTA (Schaap et al, 2001) predicted VGM soil hydraulic parameters.

parameter	description	unit	mean	standard deviation	correlation coefficients θ_r	θ_s	$\log_{10}(\alpha)$	$\log_{10}(n)$	$\log_{10}(K_\mathrm{s})$
θ_r	res. water content	$\mathrm{cm^3cm^{-3}}$	0.0577	0.0153	1.00				
θ_s	sat. water content	$\mathrm{cm^3cm^{-3}}$	0.4337	0.0159	0.09	1.00			
$\log_{10}(\alpha)$	shape parameter	$\mathrm{cm^{-1}}$	-2.2719	0.0748	0.15	0.24	1.00		
$\log_{10}(n)$	shape parameter	-	0.2146	0.0140	-0.58	-0.04	-0.86	1.00	
$\log_{10}(K_\mathrm{s})$	sat. permeability	cm/day	1.4386	0.3063	-0.97	0.12	-0.10	0.57	1.00

quantify the impact of bedrock depth and soil hydraulic uncertainty on the simulated values and confidence intervals of FS. We assume constant (Table 2) values for the shear strength parameters in all our numerical simulations. Keeping shear strength parameters constant allows us to better understand the influence of the geologic condition and soil hydraulic parameters.

Table 2: Geotechnical parameters assumed in this work.

type	parameter	value	unit
soil and water properties	γ_w	10	kN/m^3
	γ_nat	18	kN/m^3
	γ_sat	20	kN/m^3
strength parameters	c'	5	kPa
	ϕ'	30	$\circ$
	ϕ_b	15	$\circ$

Numerical solution of Richards' equation was obtained by imposing a precipitation water flux, Q (L/T), across the surface boundary (Γ) as follows, that is, $\nabla \cdot [K(\psi)\nabla(\psi)] = Q(x, y, z, t)$ at Γ (see Figure 2).

We can summarize the main capabilities of our program in three different case studies: the impact of bedrock depth uncertainty (case 1), soil hydraulic uncertainty (case 2), and both sources simultaneously (case 3) on the simulated values of ψ, FS, collapse mechanisms and probability of failure. Table 3 summarizes the case studies used in this paper to test the Monte Carlo approach. Slope geometry and soil hydraulic parameters were presented in sections 3.2 and 3.3, respectively.

Table 3: Summary of the case studies used in this paper.

case	source of uncertainty: bedrock surface	hydraulic parameters
1	$\boldsymbol{\hbar}$	$\boldsymbol{\mu_p}$
2	$\mathbb{E}(\boldsymbol{\hbar})$	$\mathcal{N}(\boldsymbol{\mu_p}, \boldsymbol{\Sigma_p})$
3	$\boldsymbol{\hbar}$	$\mathcal{N}(\boldsymbol{\mu_p}, \boldsymbol{\Sigma_p})$

The code here developed runs the Richards' solver in parallel. In this multi-core implementation, different bedrock surfaces or soil hydraulic parameters are evaluated simultaneously in parallel using distributed computing toolbox of MATLAB. This reduces considerably the computational burden, since the Richards' solver is often computationally demanding. Serial implementation is used for the NLA code.

5 POST-PROCESSING TOOLS

Figure 5 shows results of the transient variation of FS for the case 1 (see Table 3). The mean FS is represented by red line and the gray regions depict 95% confidence intervals. The FS values for two samples, $\mathbf{H}_a$ and $\mathbf{H}_b$, with different bedrock surfaces are also exhibited. The measured hyetograph (bar plot of the left axis) displays three individual storm events (days 2-4, days 7-13 and days 18-21), used as our boundary condition, Q, for the Richards' solver. The last of these three events exhibits the largest intensity and volume of rainfall. Four vertical dashed blue lines represent different saturation conditions. The samples $\mathbf{H}_a$ and $\mathbf{H}_b$ resulted in different values of FS. In this simulation soil hydraulic parameters were constant, thus the difference in FS is due to the shape of the soil-bedrock interface.

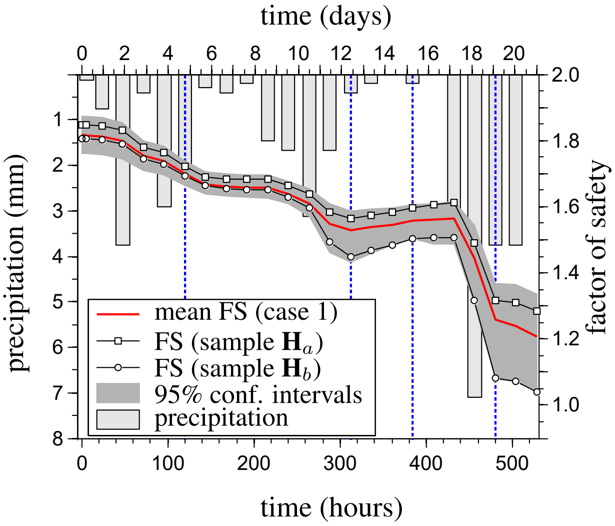

Figure 5: Transient variation of FS (right axis) predicted for the case 1 (uncertainty of the soil-bedrock interface). The red line represent the mean FS values and the gray regions depict 95% confidence intervals. The samples $\mathbf{H}_a$ and $\mathbf{H}_b$ have different bedrock surfaces. The hyetograph (left axis) represents atmospheric boundary condition used. Blue vertical lines are time steps analyzed.

Figure 6 provides the coefficient of variation of the factor of safety ($\mathrm{COV}_{\mathrm{FS}}$) with time for the three case studies. Our results of course agree well with the confidence intervals for the factor of safety (Figure 5). While $\mathrm{COV}_{\mathrm{FS}}$ for the cases 1 and 2 are relatively similar, case 3 shows a systematic increase in $\mathrm{COV}_{\mathrm{FS}}$. This finding clearly demonstrates the role played by the bedrock depth uncertainty on the reliability of landslide stability.

Figure 7 exhibits a post-processing plot of the ψ distribution in the soil-bedrock interface (a, b, c, d), ψ distribution along the transect **CC'** (e, f, g, h) and velocity vectors at collapse of the slope (i, j, k, l) for the sample $\mathbf{H}_a$. Four different time steps (indicated in Figure 5) represent distinct saturation conditions. Depth to bedrock not only controls the distribution of pore pressure, but also influences regions of intense plastic shearing (red arrows in (i), (j), (k), (l) plots). In fact, the loss of suction for $t = 120$ h (e) brings the development of a circular failure near the top of the slope (i). When the soil-bedrock interface becomes saturated, near a thin regolith zone (f, g, h), the regions of plastic shearing now develop at these high pore pressure zones (j, k, l).

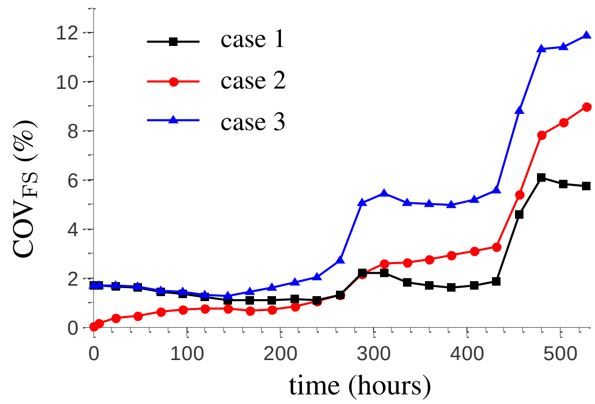

Figure 6: Transient behavior of coefficient of variation of the factor of safety ($\mathrm{COV}_{\mathrm{FS}}$) for the three case studies. This plot displays larger $\mathrm{COV}_{\mathrm{FS}}$ for the case 3.

The shape of the probabilistic distribution of the factor of safety (not shown) and the corresponding coefficient of variation (Figure 6) provide a means for evaluating two alternative measures of safety: the reliability index (β) and the probability of failure (P_{f}). Mathematical formulas for both metrics are readily found in geotechnical textbooks. Table 4 shows P_{f}-values for the three different case studies. We consider the actual probabilities for three different time steps. Based on the statistics presented, we can conclude that the combined effect of uncertainties (bedrock depth and hydraulic properties) must be explicitly evaluated in probabilistic simulations of slope stability. Indeed, P_{f}-values for the case 3 (last column) is always higher than the other cases. Therefore, if the uncertainty ranges of the bedrock depth are neglected, our study suggests that the reliability analysis can be inappropriately unconservative.

Table 4: Probabilities of failure based on log-normal distribution of FS for the three case studies.

	P_{f} (%)		
time (h)	case 1	case 2	case 3
480	0.01	0.08	1.81
504	0.01	0.37	2.59
528	0.06	1.36	4.98

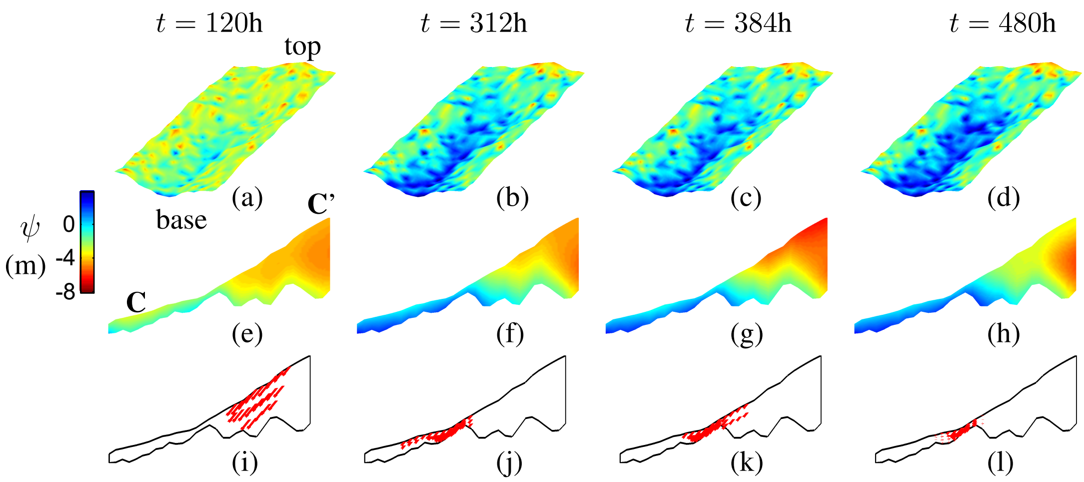

Figure 7: Post-processing plot showing the pressure head distribution in the soil-bedrock interface (a, b, c, d), pressure head along the transect **CC'** (e, f, g, h) and velocity vectors at collapse of the slope (i, j, k, l). Four different time steps represent distinct saturation conditions.

6 CONCLUSIONS

The integrated computer program presented herein enables explicit treatment of uncertainty in key inputs of slope stability models of unsaturated soils. By using the designed Monte Carlo approach, the effects of uncertainty of the bedrock surface (case 1), soil hydraulic parameters (case 2) and the combination of both (case 3) were evaluated through the confidence intervals of the factor of safety, coefficient of variation and probability of failure.

Bedrock depth uncertainty improves significantly the quantification of prediction intervals for the FS. One of the major strengths of our proposed method is that, instead of merely assuming a known and deterministic bedrock surface, one can propagate the effects of the uncertainties in the geotechnical analysis.

The MATLAB toolbox of the integrated unsaturated flow and numerical limit analysis is available upon request from the first author. This includes the setups and modeling scripts of the examples used in this paper.

REFERENCES

Camargo, J.T.; Velloso, R.Q. and Vargas Jr., E.A. (2016). Numerical Limit Analysis of Three-dimensional Slope Stability Problems at Catchment Scale, *Acta Geotechnica*, p. 1–15.

Duncan, J.M. and Wright, S.G. (2005). *Soil Strength and Slope Stability*, John Wiley & Sons, New York, NY, USA, Vol. 2, 297 p.

Gomes, G.J.C.; Araújo, J.P.; Vargas Jr., E.A.; Fernandes, N.F. (2016a). In-situ regolith depth measurements by DPL tests, *XVIII Braz. Conf. on Soil Mech. and Geotech. Eng.*, COBRAMSEG, Belo Horizonte, Vol. 1.

Gomes, G.J.C.; Vrugt, J.A. and Vargas Jr., E.A. (2016b). Toward Improved Prediction of the Bedrock Depth Underneath Hillslopes: Bayesian Inference of the Bottom-up Control Hypothesis using High-Resolution Topographic Data, *Water Resources Research*, Vol. 52.

Micheletto, M. (2008). *Development of Numerical Procedures for the Analysis of Infiltration and Slope Stability in Large Areas*, Master Thesis, Civil Engineering Graduate Program, Department of Civil Engineering, PUC-Rio, 152 p.

Schaap, M.G.; Leij, F.J. and van Genuchten, M.Th. (2001). ROSETTA: A Computer Program for Estimating Soil Hydraulic Parameters with Hierarchical Pedotransfer Functions, *Journal of Hydrology*, Vol. 251, p. 163–176.

Scharnagl, B.; Vrugt, J.A.; Vereecken, H. and Herbst, M. (2011). Inverse Modelling of In Situ Soil Water Dynamics: Investigating the Effect of Different Prior Distributions of the Soil Hydraulic Parameters, *Hydrology and Earth System Sciences*, Vol. 15, p. 3043–3059.

Vrugt, J.A. (2016). Markov Chain Monte Carlo Simulation Using the DREAM Software Package: Theory, Concepts, and MATLAB Implementation, *Environmental Modelling & Software*, Vol. 75, p. 273–316.